Structure Formation and Multi-layering in an Electrodeposited Copper-Antimony Alloy

V. Kostov and Ts. Dobrovolska*

Institute of Physical Chemistry, Sofia Bulgarian Academy of Sciences, 1113, Acad. G. Bonchev 11, Bulgaria
*Corresponding author: dobrovolska@eu.umicore.com

Abstract
The present study has investigated electrolysis conditions, in which spatiotemporal structures onto the cathode surface could be observed for the first time, under strictly controlled settings, during Cu-Sb alloy ED. Self-organization phenomena, such as in depth self-assembled deposits structures, appeared when Sb content was higher than 70 wt% in the coatings. The layers and their structures different optical and morphologic areas were characterized.

Keywords: Cu-Sb alloy; ED; multilayers; self-organization.

Introduction•
Cu ED obtained from acidic solutions is perhaps one of the best researched processes in electroplating, due to its tremendous technological importance and wide applications; a half century ago, in the automotive industry and, now, in semiconductors [1, 2]. It is known that bright Cu coatings cannot be obtained from simple acidic electrolytes, since the former are coarse-grained and powdery. For obtaining fine-grained coatings, organic additives are of prime importance. As a side effect of plating, these additives are destructed. It is assumed that these organic additives have a polarizing effect on Cu ED process. At the same time, they have an adsorption-desorption action, especially in the ED of micro- and nano-sized semiconducting products [1-4].

Numerous attempts have been made to avoid additives, especially in the case of thicker coatings, due to their incorporation (or parts thereof) into the Cu layer, which unfavorably alters some of its properties, for instance, increasing its hardness and worsening its ductility. Alloying with small metal amounts, in order to improve the coating brightness and reduce its grain size, is considered a successful option. For instance, a low percentage of Co or Ni provides brightness to Au plated layers [5], and 1-2% of Sb increase Ag brightness, hardness and wear resistance [6].

During Ag-Sb ED, the most vivid examples of self-organization have been observed [7-12]. This self-organization is expressed by the formation and

---

• The abbreviations and symbols definition lists are in pages 344-345.

propagation of some periodic spatiotemporal structures, both on the coating surface and depth. Clear, highly visible lamellae made of layers with different compositions and properties have been reported [10, 11]. Sb CD within a certain range acts as a brightening agent on Ag ED [7]. The hypothesis that the CD Sb may also act as a brightener in Cu deposition, similar to its action in the Ag-Sb alloy, was the focus of the present research.

In a previous work [13], a preliminary study of CD Cu and Sb from MSA electrolytes was presented. Moreover, it has been shown that CD Sb results in an increase in the layers internal stress, producing visible cracks [14]. At certain electrolysis conditions, heterogeneous coatings are obtained, indicating the initial stages of the formation of periodic structures [13, 14].

The present research had two goals: to find the electrolyte composition, as well as the electrolysis conditions under which the formation, observation and study of well-pronounced periodic structures on the electrode surface, during Cu-Sb alloy deposition, was possible; and to study the electrode processes arising during the alloy ED from MSA electrolytes, as well as the phase and morphological characteristics of the resulting coatings, depending on their composition.

Experimental

The electrolyte composition was: 40 g/L^{-1} Sb, as $K(SbO)C_4H_4O_6.0.5H_2O$; 4 g/L^{-1} Cu, as $CuSO_4·5H_2O$; 20 mL/L^{-1} MSA; and 90 g/L^{-1} $KNaC_4H_4O_6.4H_2O$. Chemical substances of pro analysis purity and distilled water were used to prepare the electrolyte.

The redox processes of the investigated electrolytes were characterized by the CV technique, at a SR (V) of 20 mV/s^{-1}.

The experiments were carried out in a three-electrode glass cell with a volume of 100 mL, at room T, without stirring the electrolyte. Pt was used for one WE (1 cm^2) and two CE (around 4 cm^2). An Ag|AgCl electrode was used as RE, of which E° with respect to the normal H electrode was 0.197 V. E° in the presented figures (X axis) was scaled vs. Ag|AgCl. The experiments were performed with a Princeton Applied Research computer-controlled model 273A potentiostat-galvanostat, with the PowerSuite corrosion research program.

Prior to deposition, the brass substrates (CuZn37), with an area of 2 x 1 cm, were degreased and subsequently dipped into 20% H_2SO_4. The coatings were deposited into a 100 cm^3 cell, at room T, under galvanostatic or potentiostat conditions, on CuZn37. The alloy coatings, with a thickness of about 1-10 μm, were deposited in the glass cell, at room T, without stirring. The alloy composition and ED rate, and the deposited coatings thickness were determined by X-RF analysis, with a Fischerscope X-RAY XDAL instrument, at 9 points (3 points each at the top, middle and bottom of the electrode). The results were taken as the average of the entire coating. Gravimetric measurements were also carried out. Sb or Cu distribution throughout the coatings surface was examined by EDS analysis.

The phase composition was characterized by X-RD, using a PANalyticalEmpyrean X-ray instrument equipped with a multichannel detector (Pixel 3D), with Cu-Kα radiation at the parameters of 45 kV/40 mA, in a 2θ range from 20 to 115°, with a scan step of 0.01°, for 20 s.

The coatings surface morphology and composition were investigated with a Carl Zeiss MERLIN microscope system, using different detectors (BSD4, HESE2, InLens and EsB), at various accelerating voltages, from 3 to 20 kV.

Cross-sections of the deposited coatings were examined by SEM, using a Tescan VEGA TS 5130 MM equipped with an EDS detector, INCAPentaFET-x3 (Oxford Instruments), for the chemical composition analysis.

Cu ions oxidation state was investigated by EPR spectra which were recorded as the first derivative of the absorption signal on a Bruker EMXplus spectrometer, within the T range from 90 to 400 K. The g-factor was determined in relation to the Mn^{2+}/ZnS standard. The signal intensity was determined by double integration.

Results and discussion

Fig. 1 presents the ED processes in the alloy electrolyte prepared in a sequence where firstly $CuSO_4$ was dissolved (curve 1), and then MSA (curve 2), $KNaC_4H_4O_6.4H_2O$ (curve 3) and MSA salt, in the form of $K_2Sb_2C_8H_4O_{12}3\ H_2O$ (curve 4), were added.
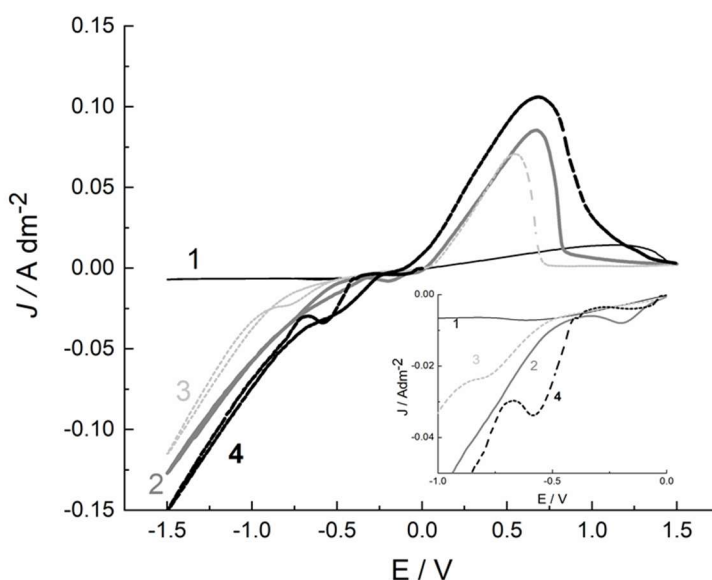
Figure 1. CV curves in the alloy electrolyte: $CuSO_4$ electrolyte (curve 1); MSA (curve 2); $KNaC_4H_4O_6.4H_2O$ (curve 3); and MSA salt in the form of $K_2Sb_2C_8H_4O_{12}\ 3\ H_2O$ (curve 4).

The initial E^o was 0 V, up to -1.5 and 1.5 V vs RE, respectively. Cu ions reduction from the aqueous solution proceeded at positive E^o (0.34 V) and, in accordance with the ions low C in the solution, at low dj (curve 1). The reduction process in the $CuSO_4$ solution (Fig. 1, curve 1) reached the maximum rate at -0.65 V (dj of 8 mA/cm^{-2}). At a more negative E^o, dj was 6 mA/cm^{-2}.

In the anodic region, a broad peak with a maximum below 1.3 V was observed. MSA addition (curve 2) significantly accelerated the cathodic process rate, which is associated with an increase in the solution acidity and HER rate. The large anodic peak, with a maximum of about 0.5 V, can be related to the larger amount of Cu deposited during the cathodic period.

It is known that the throwing power of an electrolyte is defined as the product of the solution κ and of the η derivative over $d\eta/dj$ (slope of the η-j curve) [15]. Despite that the solution κ does not linearly depend on the acidic solution C, some reasonable approximation in the diluted electrolytes might be done. MSA addition increased the solution κ, and Cu ions low C strengthened the electrical resistivity. As a result, the electrolyte macro-throwing power increased.

MSA has been used as an environmentally friendly alternative to H_2SO_4, with the main advantage of the Cu salts being more soluble in the former [16].

Cu ions oxidation state in the MSA electrolyte can be monitored by EPR studies. EPR is a convenient and sensitive method to investigate Cu (II) compounds, due to their weak spin-orbit coupling and high sensitivity (local stereochemistry and molecular motion). Also, EPR data are absolute and comparable, and their main parameters, such as g-factor and hyperfine constant, are already well-recognized in the comments on Cu complexes [17]. Fig. 2 shows Cu ions EPR spectra in an aqueous $CuSO_4$ solution without and with MSA.
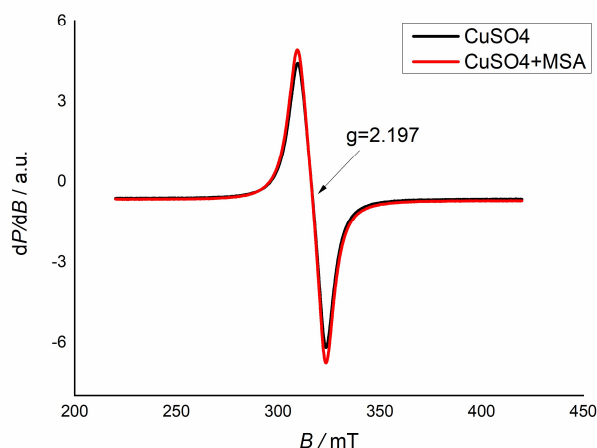
Figure 2. $CuSO_4$ solutions EPR spectra before (black curve) and after (red curve) MSA addition.

EPR spectra of both solutions show identical isotropic signals, with a giso of 2.197. This is an indication that MSA is not a complexing agent for Cu^{2+} cations. $KNaC_4H_4O_6.4H_2O$ addition (Fig. 1, curve 3) did not lead to a significant change in the cyclic curve appearance, due to the weak $C_4H_6O_6^{2-}$ ions complexing action with respect to the Cu ones [18].

$C_4H_6O_6^{2-}$ ligands addition to Cu electrolytes for electroless deposition has been practiced, but the known data are related to the neutral and alkaline electrolytes. In an acidic medium, $C_4H_6O_6^{2-}$ (which is highly protonated and, therefore, has a decreased complexation efficiency) complexing action can be judged from the data obtained from the EPR spectra.

The investigated electrolyte molar ratio of Cu ions to those of $C_4H_6O_6^{2-}$ is 1:5. The chelates formed in 1:1 Cu-$C_4H_6O_6$ solutions have been extensively investigated by EPR, in the range of pH 2 from 11. However, their structures remain unclear, due to the multi-dentate character of $C_4H_6O_6$, which can participate in polymeric

complexes, and to its several ionizable H atoms that make the complex formation very pH dependent [19].

A slight change in the g-factor, after $C_4H_6O_6^{2-}$ addition to the electrolyte, from 2.197 to 2.182, hints at the weak compound ions complexation with respect to Cu (Fig. 3). The results show a negligible change in the surrounding Cu ion, but this was important to exclude the formation of some polymeric adsorbates, which, in some cases, could be autocatalytic in the pattern formation process [12].
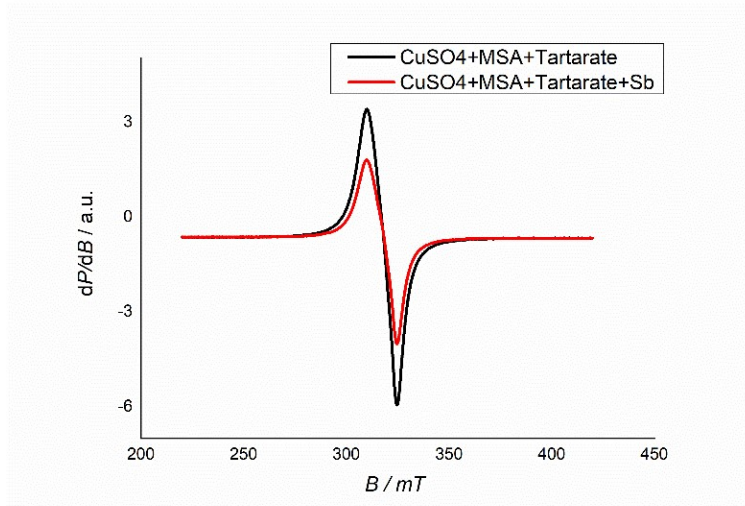
Figure 3. CuSO$_4$ and MSA solutions EPR spectra, after C$_4$H$_6$O$_6$ (black curve) and Sb (red curve) sequential addition.

CuSO$_4$ and MSA solutions EPR spectra show an anisotropic signal, with a perpendicular and parallel component (giso = 2.182).

The addition of a Sb salt, such as $K_2Sb_2C_8H_4O_{12} \cdot 3\,H_2O$, led to the appearance of a peak in the CV curve, with a maximum at -0.5 V, which corresponds to Sb deposition (Fig. 1, curve 4). The standard Sb electrode E^o of 0.212 V was clearly related to the $C_4H_6O_6^{2-}$ ions complex formation.

The coatings Sb content dependence on dj is shown in Fig. 4, where the alloy composition was determined by X-RF analysis (see experimental part).

At the lowest applied dj of 0.1 A/dm^{-2}, pure Cu was deposited. It is obvious that the coating Sb content increased very sharply, even at very low dj values, and, at 0.4 A/dm^{-2}, it reached 70 wt%. The deposition was performed within the same time (30 min). The cathodic efficiency of the process with the respective deposition rate was different: 0.05 μm/min^{-1} at 0.1 A/dm^{-2}; and 0.3 μm/min^{-1} at 0.4/A dm^{-2}.

This behavior seems to be logical, considering that Cu is the nobler metal, even in extremely small amounts in the electrolyte, meaning it was almost always deposited at the limiting dj, which, judging by the CV curve, should be in the order of 0.1-0.15 A/dm^{-2}. However, a similar course of the curve was observed at another ratio of the two metals in the electrolyte, where the Sb content also steeply increased from 0.4 to 0.5 A/dm^{-2}, which was further attributed to their very close deposition E^o in the investigated MSA-C$_4$H$_6$O$_6^{-2}$ electrolytes [14]. In all cases, the alloy deposition from MSA-C$_4$H$_6$O$_6^{-2}$ electrolytes was regular, according to the classification made by Brenner [5].
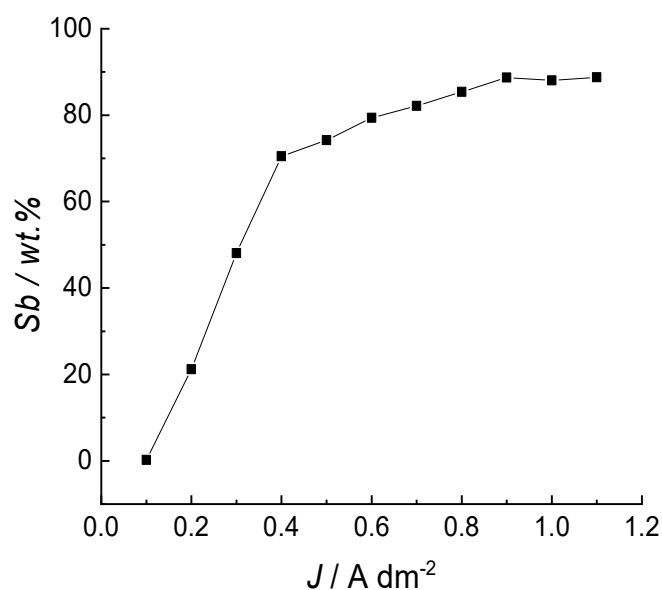
Figure 4. Sb coatings content dependence on dj.

The coatings obtained at low dj values, with Sb contents from 5 to 20 wt%, were bluish, bright and shiny. At a higher Sb content (with an average composition from 45 to 60 wt%), they were heterogeneous, with well-defined spatiotemporal structures on their surfaces. Obviously, this heterogeneity was due to Cu lattice saturation with Sb, at the formation of a solid solution, and to the transition into a spontaneous formation of a new more Sb-rich phase at higher dj values. According to the metallurgically derived Cu-Sb alloy phase diagram [20], the Cu crystal lattice saturates after reaching about 30 wt% Sb. So, the formation of phase heterogeneous coatings under these conditions is logical. The formation of spatiotemporal structures during the alloys ED fits into the process of non-linear dynamics, where the reaction-diffusion mechanism is coupled with some adsorbing effect (some autocatalytic steps).

Under certain conditions, the various Sb-rich phases on the electrode surface arranged themselves into periodic structures, such as waves, spirals and other shapes. Such cases of resulting heterogeneous coatings in the form of spiral formations are illustrated in Fig. 5.

Fig. 5 shows that Sb-rich areas are coarse grained and made up of big aggregates (up to 1 μm). Cu-rich areas have a much smoother morphology. It should be noted that the thickness of the formed complex during the different sublayers (Cu and Sb) ED was substantially smaller than the penetration depth of the electron beam during EDX analysis. As a result, the beam penetrated through several light and dark sublayers.

The comparison of the heterogeneities with the ones obtained by various other alloy systems (Ag-Sb [7-9], Ag-In, Ag-Cd, In-Co and Pd -In [21-28]) ED allowed us to suggest that this is a similar system, in which the structures appeared early in the plating process, and, during it, they moved, annihilated and reappeared with increasing coating thicknesses.
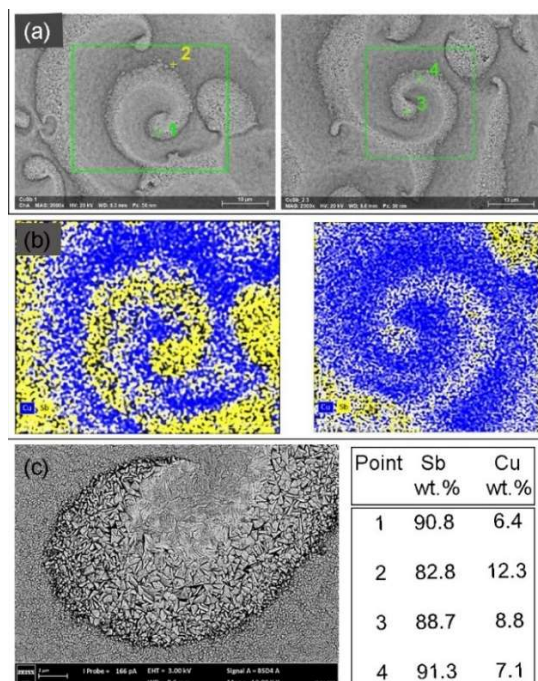
Figure 5. Heterogeneous coatings with spatiotemporal structures on the electrode surface: **a)** SEM image of the deposited coating at 0.4 A/dm^{-2}; Sb average content of 85 wt% and thickness of 8 μm; **b)** elemental mapping of Cu and Sb locally enriched on the electrode surface; and **c)** typical morphology of Sb-richer areas, with large and triangular crystallites.

Fig. 6 presents the coatings phase composition as a dj function (Sb content in the coating).
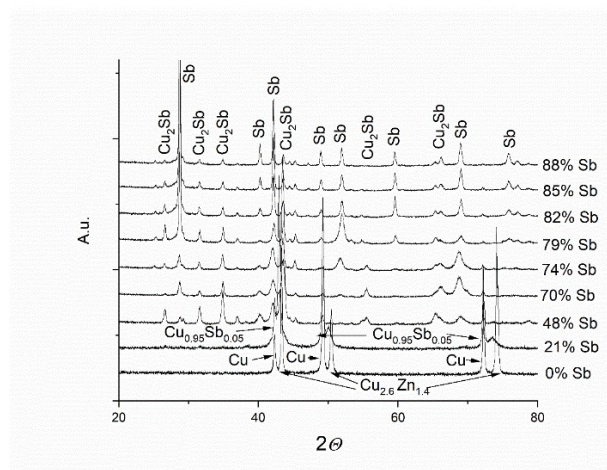
Figure 6. X-ray phase analysis of alloy coatings.

At Sb compositions up to 20 wt%, only the reflections of the Cu alpha (α) phase were observed, which is consistent with the phase diagram. The $Cu_{2.6}Zn_{1.4}$ phase recorded peaks were due to reflexes from CuZn37, on which the coatings were deposited. At 21 wt% Sb, $Cu_{0.95}Sb_{0.05}$ phase also appeared. At a higher Sb content, the reflexes of only two phases were observed, that of intermetallic Cu_2Sb and of pure Sb.

The presence of heterogeneities on the coating surface leads to the logical question: was there any evidence of coating heterogeneity in its depth?

Fig. 7 shows a cross-section of an alloy coating with a thickness of about 9 μm, of which surface structures show Cu (red), Sb (green) and C (blue) spectra in a line through the coating depth.
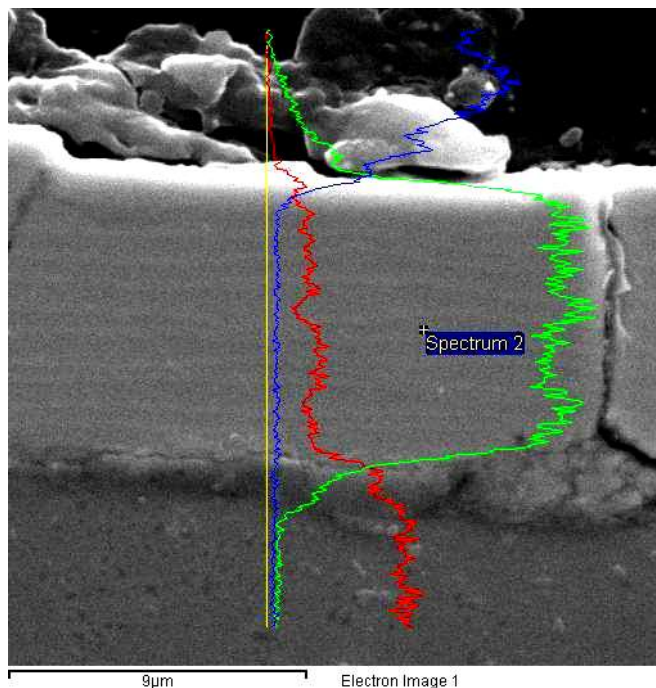
Figure 7. EDS line image of a cross-section of the Cu-Sb alloy coatings, with a thickness of 9 μm, onto CuZn37 (the sample presented in Figs. 5 and 6), which shows Cu (red), Sb (green) and C (blue) spectra.

The Cu line is of increased intensity in the resin area, in which the specimen is embedded. The signal low level indicates a probable small Cu incorporation into the K_2CO_3 coating in the electrolyte. Some very weak oscillations in Cu and Sb spectra were recorded, which may be related to the coating multi-layering, and to the small oscillations of the Sb contents in it. About ten sublayers were observed across the coating thickness. The darker sublayers are those with a richer Cu content, which are significantly thicker than the lighter ones that have a higher Sb content.

Such multilayered architecture has been seen in all coatings, where the Sb contents corresponded to more than 70 wt%. It should be noted that the same layer-by-layer morphology has also been observed during Ag ED with Sb and In, as well as of In with Co [10, 11, 26, 27], in which the top surface was covered with spatiotemporal patterns.

This multi-layered architecture must be connected with some oscillations of the process. J oscillations were observed in Ag-Sb [10, 11], but not in Ag-In [20] and In-Co [23, 28, 29] alloys ED. In Cu-Sb ED case, galvanostatic curves (E-t transient) show a single spike during the first 10 s of deposition, followed by the estimation of a constant E^o (Fig. 8).
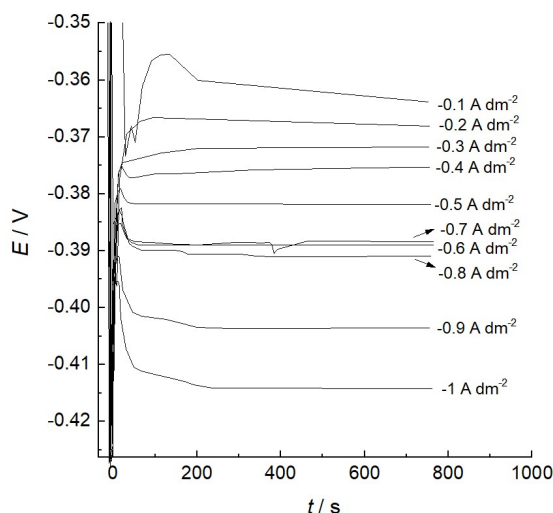
Figure 8. E-time transient recorded at the Cu-Sb alloy potentiostatic deposition from 0.1 A/dm^{-2} to 1 A/dm^{-2}, with a step of 0.1 A/dm^{-2}.

Visible oscillations could not be seen, and this is valid for dj-t transient (Fig. 9).
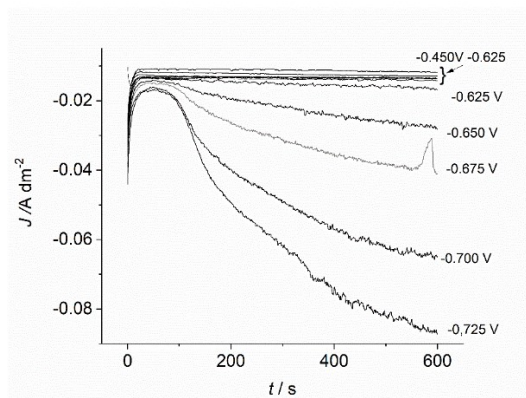
Figure 9. J-time transient recorded at the Cu-Sb alloy potentiostatic deposition from -0.475 to -0.725 mV, with 25 mV steps.

Some phenomenological explanation could be that, since Cu was deposited at a limited dj, at certain time, some Cu ions depletion happened at the double layer vicinity. A more intensive Sb ED was accompanied by an intensive HER. Due to the natural convection effect on the double layer vicinity, stirring occurred, and a new portion of the Cu ions started coming from the electrolyte bulk, restarting the Cu-reach lamellae ED process. We recall that all experiments were performed in the vertical electrode, of which natural convection was not suppressed, without stirring.

Conclusions
This research studied the electrolysis conditions in which spatiotemporal structures could be observed for the first time under strictly controlled settings, during Cu-Sb alloy ED.
Spatiotemporal structures appeared when Sb content was higher than 70 wt% in the coatings. The richer in Sb was the area, the bigger were the formed crystallites.

Most likely, the structures different optic and morphologic areas consisted of Cu_2Sb and Sb phases. As a self-organization phenomenon, deposits in depth self-assembled structure were observed, and the layers were characterized. This will allow the next steps in the investigation of the properties of this unique alloy system.

Acknowledgements

Authors' contributions
Vasil Kostov: collected the data; contributed with data or analysis tools; performed the analysis. **Tsvetina Dobrovolska**: conceived and designed the analysis; contributed with data or analysis tools; wrote the paper.

Abbreviations
Ag|AgCl: silver chloride
C: concentration
$C_4H_6O_6{}^{2-}$: tartaric acid
CE: counter electrode
$CuSO_4$: copper sulfate
$CuSO_4 \cdot 5H_2O$: copper (II) sulfate pentahydrate
CV: cyclic voltammetry
dj: current density
E^o: potential
ED: electrodeposition
EDS: energy dispersive spectroscopy
EPR: electronic paramagnetic resonance
giso: isotropic g-factor of proportionality
H_2SO_4: sulfuric acid
HER: hydrogen evolution reaction
j: current
K_2CO_3: tartar salt
$K_2Sb_2C_8H_4O_{12}3\ H_2O$: potassium antimonyl tartrate
$KNaC_4H_4O_6.4H_2O$: potassium sodium tartrate
$K(SbO)C_4H_4O_6.0.5H_2O$: antimony potassium tartarate
Mn^{2+}/ZnS: divalent manganese cation/zinc sulfide
MSA: methanesulfonic acid
RE: reference electrode
Redox: reduction and oxidation
SEM: scanning electronic microscopy
SR: scan rate

T: temperature
WE: working electrode
X-RD: x-ray diffraction
X-RF: X-ray fluorescence

Symbols definition
κ: conductance
η: overpotential

References

1. Kondo K, Akolkar RN, Barkey DP et al. Copper electrodeposition for nanofabrication of electronics devices (Vol. 171) New York: Springer. 2014.
2. Kanani N. Kupferschichten: Abscheidung, Eigenschaften, Anwendungen, Bad Saulgau: Leuze Verlag. 2000.
3. Stoychev DS, Vitanova I, Vitanov T et al. The relation between the adsorption of surface-active additives and the brightness of electrolytically deposited copper coatings. Surf Technol. 1980;10(3):209-217. https://doi.org/10.1016/0376-4583(80)90076-X
4. Mirkova L, Nanev C, Rashkov R. The role played by hydrodynamics in the levelling process during bright copper platting from acidic electrolytes. Part I. Surf Coat Technol. 1988;34(4):471-482. https://doi.org/10.1016/0257-8972(88)90102-8
5. Brenner A. Electrodeposition of alloys: principles and practice. Academic Press New York and London: 1963.
6. Krastev I, Petkova N, Zielonka A. Properties of silver–antimony alloys electrodeposited from ferrocyanide–thiocyanate electrolytes. J Appl Electrochem. 2002;32(7):811-818. https://doi.org/10.1023/A:1020125532099
7. Kristev I, Nikolova M. Structural effects during the electrodeposition of silver-antimony alloys from ferrocyanide-thiocyanate electrolytes. J Appl Electrochem. 1986;16(6):875-878. https://doi.org/10.1007/BF01006532
8. Nakabayashi S, Krastev I, Aogaki R et al. Electrochemical instability of Ag/Sb co-deposition coupled with a magnetohydrodynamic flow. Chem Phys Lett.1988;294(1-3):204-208. https://doi.org/10.1016/S0009-2614(98)00858-6
9. Nakabayashi S, Inokuma K, Nakao A et al. Colliding spiral waves propagating on the electrode. Chem Lett. 2000;29(2):88-89. https://doi.org/10.1016/S0009-2614(98)00858-6
10. Krastev I, Baumgärtner ME, Raub CJ. Stromoszillationen bei der galvanischen Absheidung: Untersuchungen zur Silber-Antimon-Legierungsabsheindung.I. Metalloberfläche 1992;46(2):63-66.
11. Krastev I, Baumgärtner ME, Raub CJ. Stromoszillationen bei der galvanischen Abscheidung: Untersuchungen zur Silber-Antimon-Legierungsabscheidung. II. Metalloberfläche 1992;46(3):115-120.
12. Krastev I and Koper MTM. Pattern formation during the electrodeposition of a silver-antimony alloy. Phys A: Statist Mec Appl. 1995;213(1-2):199-208. https://doi.org/10.1016/0378-4371(94)00161-L
13. Kostov V, Krastev I, Dobrovolska Ts. Pattern formation during electrodeposition of copper-antimony alloys. J Electrochem Sci Eng. 2016;6(1):105-111. https://doi.org/10.5599/jese.235

14. Hrussanova A, Krastev I, Zielonka A. Effect of the electrolyte composition on the electrodeposition of Cu-Sb alloys from methanesulphonate-tartrate electrolytes. Zastita materiala. 2011;52(3):145-151.

15. Wagner C. Theoretical analysis of the current density distribution in electrolytic cells. J Electrochem Soc. 1951;98(3):116. https://doi.org/10.1149/1.2778113

16. Balaji R, Pushpavanam M. Methanesulphonic acid in electroplating related metal finishing industries. Transac IMF. 2003;81(5):154-158. https://doi.org/10.1080/00202967.2003.11871526

17. Hitchman MA, Waite TD. Electronic spectrum of the hexaaquocopper (2+) ion. Inorg Chem. 1976;15(9):2150-2154. https://doi.org/10.1021/ic50163a030

18. Dean JA. Lange's Hand Book of Chemistry, New York: McGraw-Hill. 1999.

19. Chasteen N, Belford R. Triplet state of a binuclear copper dl-tartrate and electron paramagnetic resonance spectra of the copper tartrates. Inorg Chem. 1970;9(1):169-175. https://doi.org/10.1021/ic50083a033

20. Fürtauer S, Flandorfer H. A new experimental phase diagram investigation of Cu–Sb. Monatshefte für Chemie. 2012;143:1275-1287. https://doi.org/10.1007/s00706-012-0737-1

21. Dobrovolska Ts, Veleva L, Krastev I et al. Composition and structure of silver-indium alloy coatings electrodeposited from cyanide electrolytes. J Electrochem Soc. 2005;152(3):137. https://doi.org/10.1149/1.1859811

22. Dobrovolska T, López-Sauri DA, Veleva L et al. Oscillations and spatio-temporal structures during electrodeposition of AgCd alloys. Electrochim Acta. 2012;79:162-169. https://doi.org/10.1016/j.electacta.2012.06.100

23. Gutiérrez MAE, Dobrovolska T, Sauri DAL et al. Self-organization phenomena during electrodeposition of Co-In alloys. ECS Transac. 2011;36(1):275. https://doi.org/10.1149/1.3660621

24. Krastev I, Dobrovolska T. Pattern formation during electrodeposition of alloys. J Solid State Electrochem. 2013;17(2):481-488. https://doi.org/10.1007/s10008-012-1971-5

25. Bozzini B, Lacitignola D, Sgura I. Spatio-temporal organization in alloy electrodeposition: a morphochemical mathematical model and its experimental validation. J Solid State Electrochem. 2013;17(2):467-479. https://doi.org/10.1007/s10008-012-1945-7

26. Bozzini B, Amati M, Gregoratti L et al. Intermetallics as key to spiral formation in In–Co electrodeposition: a study based on photoelectron microspectroscopy, mathematical modelling and numerical approximations. J Phys D: Appl Phys. 2015;48(39):395502.

27. Golvano-Escobal I, Özkale B et al. Self-organized spatio-temporal micropatterning in ferromagnetic Co–In films. J Mater Chem C. 2014;2(39):8259-8269. https://doi.org/10.1088/0022-3727/48/39/395502

28. Bozzini B, Amati M, Dobrovolska Ts et al. Depth-dependent scanning photoelectron microspectroscopy unravels the mechanism of dynamic pattern formation in alloy electrodeposition. J Phys Chem C. 2018;122(28):15996-16007. https://doi.org/10.1021/acs.jpcc.8b01267

29. Golvano-Escobal I, de Dios Sirvent J, Ferran-Marqués M et al. Cross-sectioning spatio-temporal Co-In electrodeposits: Disclosing a magnetically-patterned nanolaminated structure. Mat Des. 2017;114:202-207. https://doi.org/10.1016/j.matdes.2016.11.088